

Noncontact Three-Dimensional Mapping and Ablation of Upper Loop Re-Entry Originating in the Right Atrium

Ching-Tai Tai, MD, Jin-Long Huang, MD, Yung-Kuo Lin, MD, Ming-Hsiung Hsieh, MD, Pi-Chang Lee, MD, Yu-An Ding, MD, Mau-Song Chang, MD, Shih-Ann Chen, MD

Taipei, Taiwan, Republic of China

OBJECTIVES	This study was aimed at delineating the reentrant circuit of right atrial (RA) upper loop re-entry using noncontact three-dimensional mapping.
BACKGROUND	Various forms of atypical atrial flutter including lower loop re-entry and left atrial flutter have been demonstrated. However, little is known about upper loop re-entry in the RA.
METHODS	The study population consisted of eight patients (65 ± 12 years, seven men) with atypical atrial flutter. Right atrial activation during atrial flutter was visualized using a noncontact mapping system (EnSite-3000 with Clarity Software, St. Paul, Minnesota) for a three-dimensional reconstruction of the endocardial depolarization. The narrowest part of the re-entrant circuit was targeted using radiofrequency catheter ablation.
RESULTS	Noncontact mapping showed macro-re-entry confined to the RA free wall with RA activation time accounting for 100% of the cycle length (214 ± 21 ms) in all eight patients. Two patients had counterclockwise activation, and six patients had clockwise activation around the central obstacle, which was composed of the crista terminalis, the area of functional block, and superior vena cava. The lower turn-around points were located at the conduction gap in the crista terminalis. Radiofrequency linear ablation of the conduction gap in the crista terminalis was performed and eliminated atrial flutter in six patients without recurrence during a follow-up of 3.2 ± 1.1 months.
CONCLUSIONS	Atypical atrial flutter could arise from upper loop re-entry in the RA with conduction through the gap in the crista terminalis. Radiofrequency linear ablation of the conduction gap was effective in eliminating this atrial arrhythmia. (J Am Coll Cardiol 2002;40:746–53) © 2002 by the American College of Cardiology Foundation

Typical atrial flutter has been well demonstrated as a macro-re-entrant circuit around the tricuspid annulus (1–4). Radiofrequency (RF) catheter ablation of the cavotricuspid isthmus (CTI) is highly effective in eliminating this tachycardia. However, various forms of nonincisional atypical atrial flutter have been reported, including CTI-dependent lower loop re-entry and CTI-independent right atrial (RA) and left atrial free wall flutters (5–8). Using electroanatomic mapping, Kall et al. (6) found a specific type of atypical atrial flutter arising in the RA free wall anterior to the crista terminalis. Yang et al. (8) observed upper loop reentry in the RA, but they did not elucidate the entire re-entrant circuit. Until now, noncontact three-dimensional mapping of atypical atrial flutter has not been reported.

In this study we described the electrophysiologic characteristics and results of RF ablation in a series of patients with upper loop re-entry around the crista terminalis using noncontact three-dimensional mapping.

METHODS

Patient characteristics. In 150 consecutive patients with clinically documented atrial flutter referred for RF catheter ablation, eight (5.3%) patients (seven men and one woman, 65 ± 12 years old) were found to have typical and atypical RA flutter (Table 1). These eight patients constituted the study population. One patient had received CTI ablation for typical atrial flutter. Three patients had a history of paroxysmal atrial fibrillation. Six patients had cardiovascular diseases, including two with coronary artery disease, three with hypertension, and one with rheumatic heart disease.

Catheter position. Informed written consent was obtained from all patients. As described previously, all antiarrhythmic drugs were discontinued for at least five half-lives before the study (3,9). In all patients a 7F, 20-pole, deflectable Halo catheter with 10 mm paired spacing (Cordis-Webster Inc., Baldwin Park, California) was positioned around the tricuspid annulus to record the RA activation in the lateral wall and the low RA isthmus simultaneously. A 7F, deflectable, decapolar catheter with 2-mm interelectrode distance and 5-mm space between each electrode pair was also inserted into the coronary sinus via the internal jugular vein. The position of the proximal electrode pair at the ostium of the coronary sinus was confirmed with contrast injection. A 9F sheath placed in the left femoral vein was used to introduce the noncontact mapping catheter.

From the Division of Cardiology, Department of Medicine, National Yang-Ming University School of Medicine, Taipei Veterans General Hospital, Taipei, Taiwan. Supported, in part, by grants from National Science Council (NSC 90-2314-B-010-023, 90-2314-B-075-044, 90-2315-B-010-004), Taipei, Taiwan, and Endocardial Solutions, Inc., St. Paul, Minnesota.

Manuscript received January 30, 2002; revised manuscript received May 10, 2002, accepted May 23, 2002.

Abbreviations and Acronyms

CTI	= cavotricuspid isthmus
ECG	= electrocardiogram
MEA	= multiple electrode array
RA	= right atrium
RF	= radiofrequency
SVC	= superior vena cava

Noncontact mapping system. The noncontact mapping system (EnSite 3000, Endocardial Solutions, St. Paul, Minnesota) was described in detail previously (10). In brief, the system consists of a noncontact catheter (9F) with a multielectrode array (MEA) surrounding a 7.5-ml balloon mounted at the distal end. Raw data detected by the MEA is transferred to a silicon graphics workstation via a digitized amplifier system.

Before deployment of the MEA, patients were given 3,000 IU heparin boluses to maintain activated clotting time between 250 s and 300 s throughout the study. The MEA catheter was deployed over a 0.035-in. guidewire, which had been advanced to the superior vena cava (SVC) (Fig. 1). The system locates any catheter in relation to the MEA using a “locator” signal, which serves two purposes. It is used to construct a three-dimensional computer model of the virtual endocardium providing a geometry matrix for the inverse solution. Geometric points are sampled at the beginning of the study during sinus rhythm or atrial flutter. The locator signal is also used to display and track the position of the catheter on the virtual endocardium and allows marking of anatomic locations identified using fluoroscopy and electrogram characteristics.

Using mathematical techniques to process these potentials, the system is able to reconstruct more than 3,000 unipolar electrograms simultaneously and superimpose them onto the virtual endocardium, producing isopotential maps with a color range representing voltage amplitude. Reconstructed electrograms can also be selected from sites on the virtual endocardium and displayed individually. Morphologic components in the virtual electrogram correlate with contact electrogram as previously validated (10).

Electrophysiologic study. If spontaneous atrial flutter was found at the onset of study, multicatheter mapping and noncontact mapping were performed simultaneously to investigate the reentrant circuit. If sinus rhythm was present at baseline, low RA or coronary sinus pacing was performed until 2 to 1 atrial capture was attained to induce atrial flutter. At baseline, counterclockwise typical atrial flutter was spontaneous in three patients and induced in four patients. Clockwise typical atrial flutter was induced in two of seven patients. After successful ablation of typical atrial flutter with creation of bidirectional isthmus conduction block, the previous pacing protocol was repeated (9). Sustained atypical atrial flutter was induced in all of these seven patients. The remaining one patient had induced atypical atrial flutter only.

Definitions. Anatomical nomenclature was used that reflected the true orientation and positioning of the human heart in the thorax. Using this format the SVC and RA appendage are superior, and the inferior vena cava and the CTI are inferior to the tricuspid annulus. The His bundle is positioned in the anterosuperior aspect of the medial tricuspid annulus, the coronary sinus in the posteroinferior aspect of the medial tricuspid annulus, and the crista terminalis is located in the lateral wall of the RA and is oriented from superior to inferior.

Typical atrial flutter was defined as a macro-re-entrant atrial tachycardia circulating around the whole tricuspid annulus with concomitant activation through the posterior and anterior free walls as well as conduction block along the crista terminalis.

Atypical atrial flutter was defined as any macro-re-entrant atrial tachycardia except typical atrial flutter and not produced by prior atriotomy.

Counterclockwise upper loop re-entry was defined as an atypical atrial flutter involving the upper portion of the RA with a descending activation sequence in the free wall anterior to the crista terminalis.

Clockwise upper loop re-entry was defined as an atypical atrial flutter involving the upper portion of the RA with an ascending activation sequence in the free wall anterior to the crista terminalis.

Table 1. Clinical and Electrophysiologic Data

Patient	Age, yrs	Gender	SHD	AF History	FCL, ms				INF P in ULR	RF Pulse, n	Recurrence
					CCW Typical	CW Typical	CCW ULR	CW ULR			
1	79	M	No	No	284	—	238	—	+	6	No
2	75	M	CAD	Yes	305	—	220	—	+	7	No
3	54	M	No	No	190	—	—	180	+	—	—
4	75	M	CAD	Yes	245	—	—	192	+	8	No
5	75	M	HCVD	No	205	190	—	208	—	7	No
6	61	M	HCVD	No	238	225	—	230	—	2	No
7	47	M	HCVD	Yes	—	—	—	205	+	6	No
8	57	F	RHD	No	235	—	—	230	—	—	—

AF = atrial fibrillation; CAD = coronary artery disease; CCW = counterclockwise; CW = clockwise; FCL = flutter cycle length; HCVD = hypertensive cardiovascular disease; INF = inferior electrocardiogram leads; P = P waves; RF = radiofrequency; RHD = rheumatic heart disease; SHD = structural heart disease; ULR = upper loop re-entry.

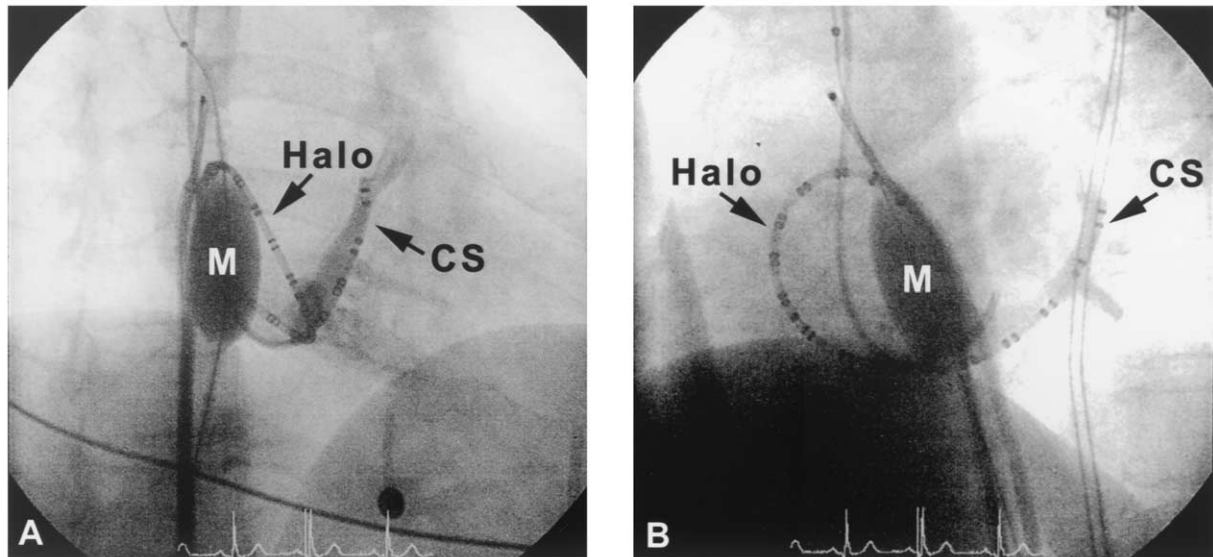


Figure 1. Radiographs showing a multielectrode array balloon catheter (M) in the right atrium, a Halo catheter around the tricuspid annulus, and a decapolar catheter in the coronary sinus (CS). (A) Right anterior oblique view. (B) Left anterior oblique view.

Conduction gap in the crista terminalis was defined as the remnant of conducting tissue bounded on both sides by regions of conduction block as determined from the isopotential map.

Double potentials were defined for conventional bipolar and virtual unipolar atrial electrograms with two discrete deflections per beat either separated by an isoelectric baseline or a low amplitude interval (11).

Scar zones were defined as areas with the amplitude of unipolar peak negative potential between 0 and -1.0 mV with slow conduction or conduction block as determined from the isopotential map.

Atypical atrial flutter ablation and follow-up. Radiofrequency ablation was performed using a 4-mm electrode-tipped ablation catheter connected to an EPT-1000 generator. The critical isthmus for the reentrant circuit was targeted. Energy applications (50W, 60°C , 40 s) were performed sequentially to produce a linear lesion. After ablation, burst pacing was performed from the low RA and coronary sinus to 2 to 1 atrial capture. Successful ablation was defined as bidirectional conduction block along the crista terminalis shown by noncontact mapping and inability to reinduce atrial flutter. After hospital discharge all patients were followed up closely in the outpatient clinic. Long-term efficacy was assessed clinically on the basis of the resting surface electrocardiogram (ECG), 24-h Holter monitoring, and clinical symptoms.

Statistical analysis. Continuous data are expressed as mean \pm SD.

RESULTS

Induction and noncontact mapping. In all eight patients, sustained atypical atrial flutter was induced with burst pacing at cycle lengths of 200 to 250 ms from the proximal coronary sinus. Spontaneous transitions between atypical

atrial flutter and atrial fibrillation were observed in three patients. The mean cycle length of atypical atrial flutter was 214 ± 21 ms. The ECGs of induced and previously documented atrial flutter were similar. The flutter waves in the inferior ECG leads were positive in five patients with distal to proximal coronary sinus activation and negative in three patients with proximal to distal coronary sinus activation (Table 1). There was no relationship between the flutter wave morphology in the inferior ECG leads and the direction of upper loop re-entry.

During sustained atypical atrial flutter, RA activation was earlier than coronary sinus activation. Noncontact mapping showed macro-re-entry confined to the RA free wall with RA activation time accounting for 100% of the cycle length in all eight patients. In the left anterior oblique view, there was counterclockwise activation in two patients and clockwise activation in six patients. In two patients with counterclockwise upper loop re-entry, the activation wavefront propagated down the anterior free wall and split into two wavefronts. One crossed the gap of the midcrista terminalis and proceeded up the posterior wall and around the central obstacle, which was composed of the upper crista terminalis, the area of functional block and the SVC, to complete the re-entrant circuit; the other approached the lateral CTI with conduction blocked at the previous ablation line for typical atrial flutter (Fig. 2). Interestingly, one patient had the area of functional block anterior to the crista terminalis and the other had the area of functional block posterior to the crista terminalis. In six patients with clockwise upper loop re-entry, the activation wavefront propagated down the posterior wall and split into two wavefronts. One crossed the gap in the crista terminalis and proceeded up the anterior free wall and around the central obstacle, which was composed of the upper crista terminalis, the area of functional block

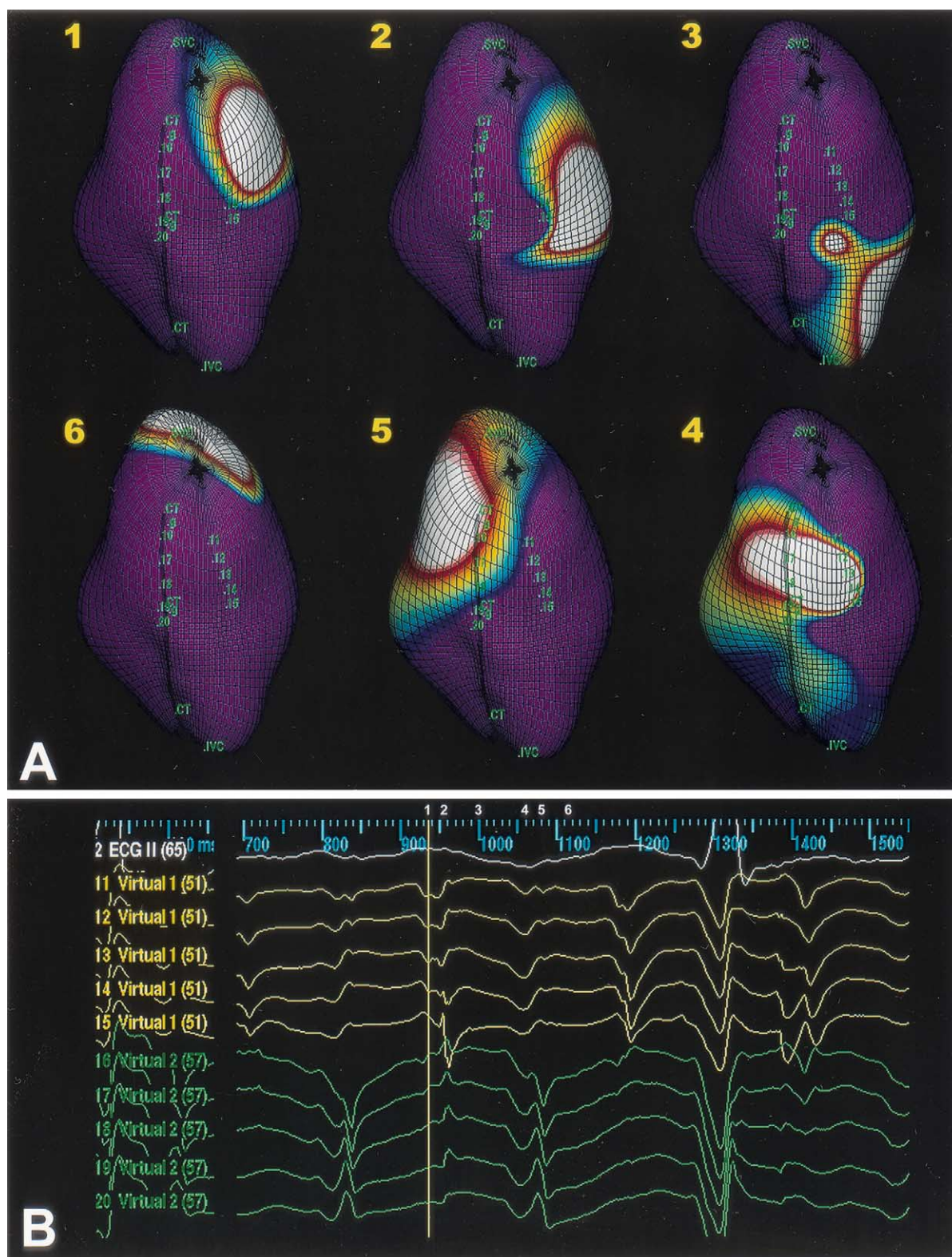


Figure 2. (A) Isopotential maps showing the activation sequence (frames 1 to 6) of counterclockwise upper loop re-entry in the right posterior oblique view. Color scale for each isopotential map has been set so that **white** indicates most negative potential and **blue** indicates least negative potential. The activation wavefront propagates down the anterolateral right atrium (RA) near the superior vena cava (SVC) (**frame 1**) to the middle and inferior anterolateral RA (**frame 2**), then splits into two wavefronts (**frame 3**); one passes around the area of functional block, and the other passes through the cavotricuspid isthmus. The wavefront in the lateral RA continues through the gap (g) in the crista terminalis (CT) (**frame 4**) to the superior posterior RA (**frame 5**) and activates the atrial wall surrounding the SVC before reactivation of the anterolateral RA once again. (B) The virtual electrograms from the area of functional block (virtual 11 to 15) and the CT (virtual 16 to 20) including the conduction gap (virtual 16 to 18) demonstrate double potentials. The **numbers 1 to 6** represent the time points at which the isopotential maps have been displayed in A. IVC = inferior vena cava.

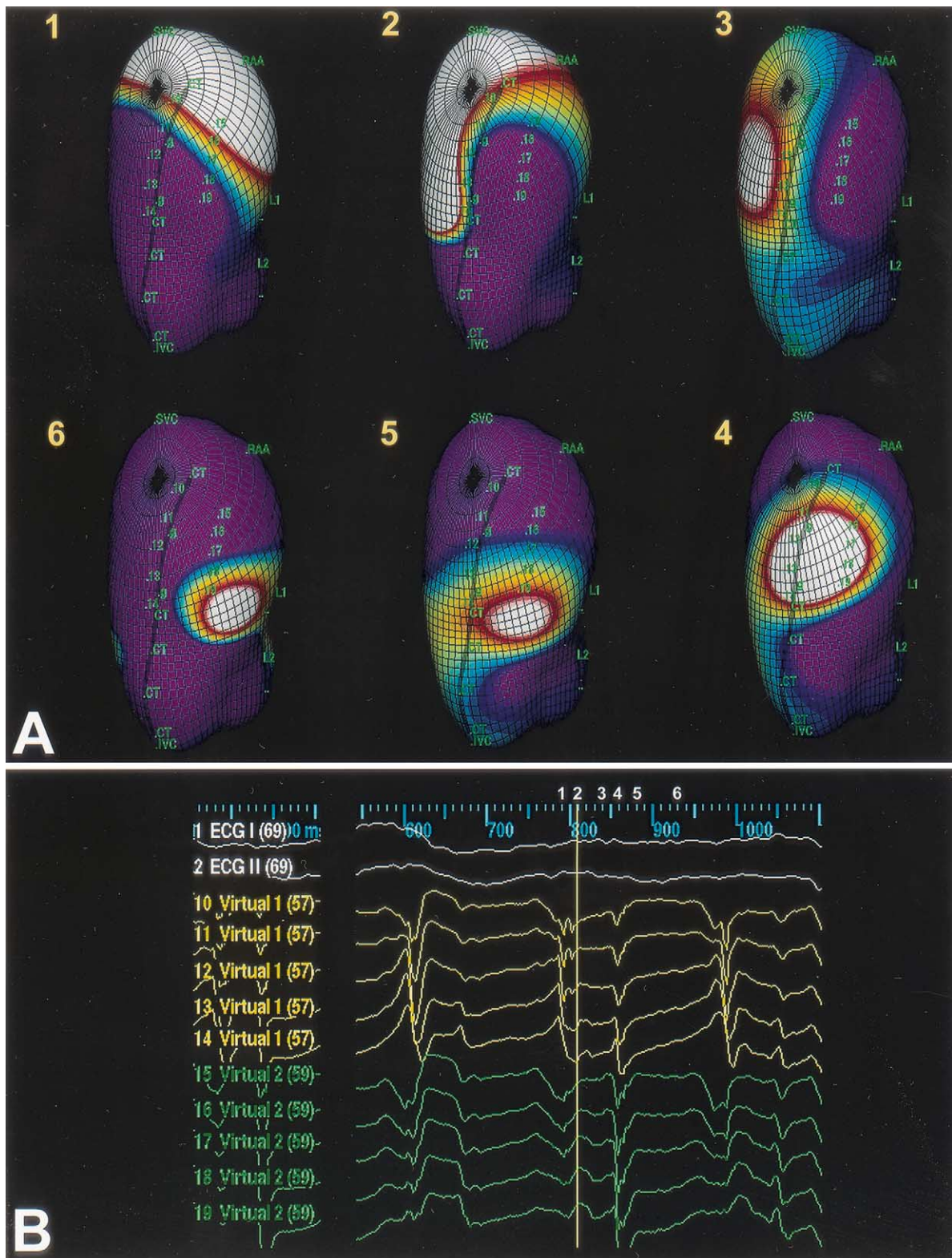


Figure 3. (A) Isopotential maps showing the activation sequence (frames 1 to 6) of clockwise upper loop re-entry in the right posterior oblique view. Color scale for each isopotential map has been set so that **white** indicates most negative potential and **blue** indicates least negative potential. The activation wavefront propagates backward and downward from the superior anteromedial right atrium (RA) near the RA appendage (frame 1) to the middle posterior RA (frame 2), then splits into two wavefronts; one passes close to the crista terminalis (CT) (frame 3), and the other passes through the septal RA (it is not shown in the figure). The wavefront in the posterior RA continues through the gap (g) in the CT (frame 4) to the lateral RA and around the area of functional block (frame 5), then activates the anterolateral RA (frame 6) before reactivation of the superior anteromedial RA once again. (B) The virtual electrograms from the CT (11 to 14) and the area of functional block (15 to 19) demonstrate double potentials. The numbers 1 to 6 represent the time points at which the isopotential maps have been displayed in A. IVC = inferior vena cava; SVC = superior vena cava.

and the SVC, to complete the reentrant circuit; the other approached the medial CTI with conduction blocked at the previous ablation line for typical atrial flutter (Fig. 3).

In all eight patients, virtual electrograms showed widely split double potentials in the crista terminalis, as well as in areas of functional block, and low amplitude potentials with fractionation at the gap in the crista terminalis during atrial flutter. During sinus rhythm areas of functional block demonstrated wide and low-amplitude potentials consistent with scar formation in two patients and normal atrium in six patients.

RF ablation and follow-up. The ablation procedure did not proceed in two patients because they felt pain during energy application. Thus, RF energy was applied sequentially on the gap in the crista terminalis during sinus rhythm in only six patients. The mean number of RF energy applications was 6 ± 2.1 . After ablation, conduction block at the gap in the crista terminalis was confirmed by atrial pacing during sinus rhythm (Fig. 4). There was no complication during the ablation procedure. During a follow-up of 3.2 ± 1.1 months, none of eight patients had recurrence of typical or atypical atrial flutter. In three patients with a history of atrial fibrillation, there has been no recurrence of atrial fibrillation during the follow-up period.

DISCUSSION

Major finding. This study demonstrated that atypical right atrial flutter could arise from upper loop re-entry around the combined anatomic and functional central obstacle. The lower turn-around point was located at the conduction gap of the crista terminalis in all eight patients. Radiofrequency linear ablation of this conduction gap was effective in eliminating upper loop re-entry in the RA.

Previous experimental and clinical atypical RA flutters. Several experimental models of right atrial atypical atrial flutter have been described (12–15). In the canine sterile pericarditis model, Shimizu et al. (12) showed that, after induction of unidirectional conduction block in the upper or lower portion of the sulcus terminalis, counterclockwise or clockwise atrial flutter could develop in the RA free wall respectively (12); the re-entrant circuit of this atrial flutter is similar to that of upper loop re-entry in this study. In the other canine sterile pericarditis model, Schoels et al. (13) demonstrated that the induced atrial flutter was single-loop re-entry around an arc of block close to the atrioventricular ring or around a combined functional and anatomic obstacle when the arc joined an atrial vessel. Similar circus movement atrial flutters were also found in the canine RA enlargement model (14,15).

In a series of 28 patients with 36 episodes of atypical right atrial flutter, Yang et al. (8) found that 67% of 36 episodes was CTI-dependent lower loop re-entry, 22% was upper loop re-entry, and 11% was macro-re-entry around low voltage areas (scars) in the posterolateral RA. They speculated that upper loop re-entry was the converse of lower loop

re-entry with a clockwise circuit and break over the lateral or anterolateral annulus with impulse collision in the CTI, but the precise path and boundaries of the circuit were not defined. Kall et al. (6) reported six patients with atypical atrial flutter originating in the RA free wall; the electroanatomic mapping demonstrated clockwise or counterclockwise activation around the vertical central line of block, which was located anterior to the crista terminalis with the length of 2.0 cm to 2.4 cm.

In the present study, we first used noncontact three-dimensional mapping to delineate upper loop re-entry in the RA and found that this circus movement tachycardia was different from previously described atypical atrial flutters, showing activation around the central obstacle, which was composed of the crista terminalis, the area of functional block and the SVC. The difference of the mechanism for atypical RA flutter between the study by Kall et al. (6) and ours lies in the role of the crista terminalis. In the Kall et al. (6) study, the crista terminalis was a barrier for the re-entrant circuit, but in our study a portion of the crista terminalis was included in the central obstacle of the re-entrant circuit because of wavefront propagation through the gap.

Role of the crista terminalis in development of atypical atrial flutter. The crista terminalis has been demonstrated to be a posterior barrier and a line of block in typical atrial flutter (1). Furthermore, limited transverse conduction capabilities of the crista terminalis may contribute to the development of typical atrial flutter (16–18). However, the rate-dependent conduction block of the crista terminalis was shown, suggesting that the line of block during typical atrial flutter was functional (16–18). In some patients complete transverse block of the crista terminalis was not achieved even during pacing until 2 to 1 atrial capture or extrastimulation with a short coupling interval (17,18). This finding suggested the presence of a transverse conduction gap in the crista terminalis, especially in patients with atrial fibrillation (18). Why conduction persists in the gap with block in the residual portions of the crista terminalis is unclear. However, the success or failure of propagation is determined by the underlying source-sink relation, which reflects a complex interaction of several factors such as tissue anisotropy, gap junction distribution, and wavefront curvature (12). Thus, the inhomogeneous conduction properties of the crista terminalis provide a predisposition to unidirectional block and induction of circus movement atrial flutter around the crista terminalis as shown in the present study.

In addition, a scar zone was combined with the crista terminalis to become the central obstacle during upper loop re-entry in two of eight patients. During sinus rhythm, the unipolar virtual electrograms in the scar zone demonstrated wide, low-amplitude, and fractionated electrograms, suggesting a delayed and nonuniform anisotropic conduction through the diseased RA. This may be related to severe atrial fibrosis resulting from proliferation of smooth muscle cells and collagen fibers beneath the endocardial lining (19).

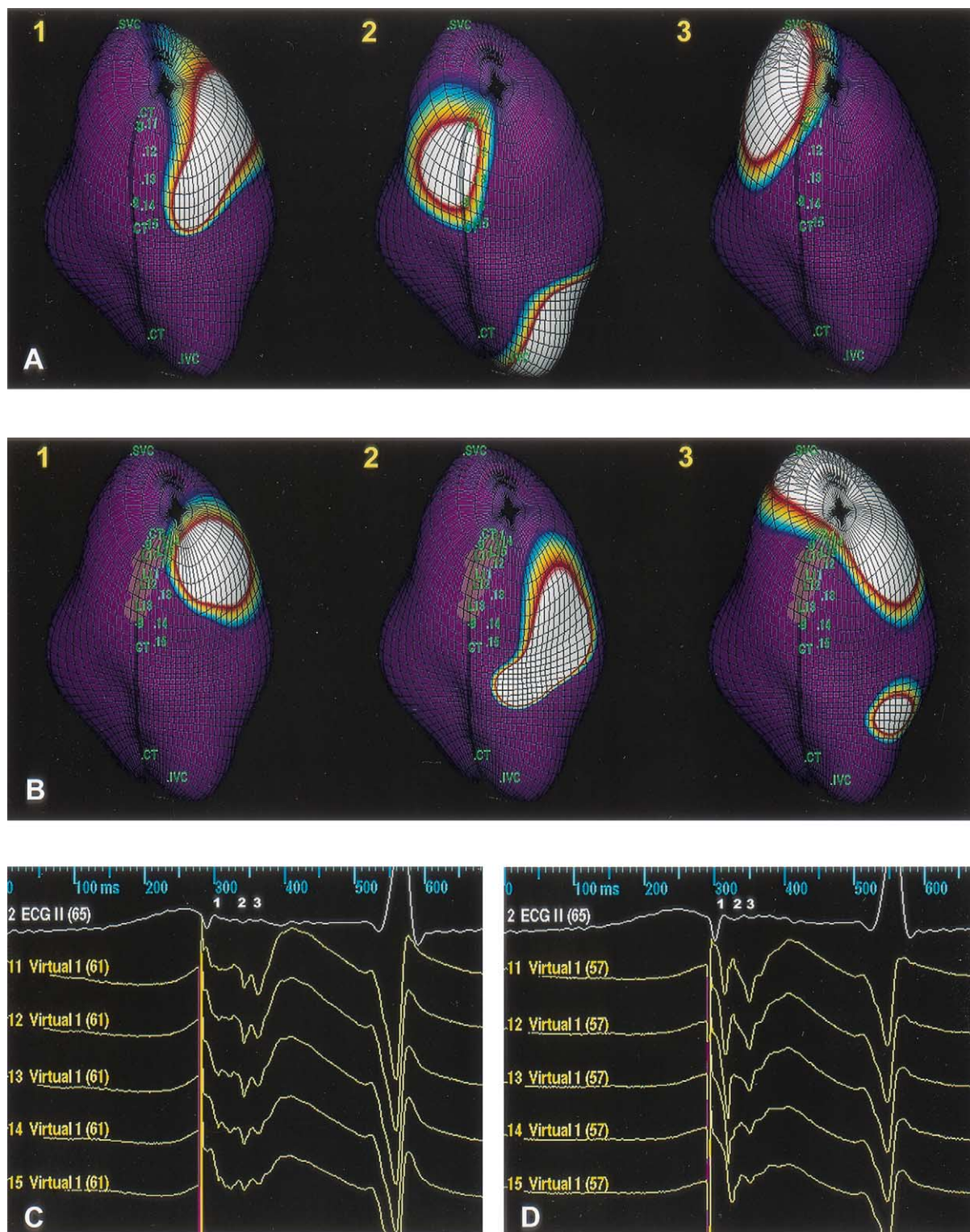


Figure 4. (A) Isopotential maps showing the activation sequence (frames 1 to 3) of atrial pacing before ablation. Color scale for each isopotential map has been set so that **white** indicates most negative potential and **blue** indicates least negative potential. The activation wavefront propagates downward from the superior anterior right atrium (RA) (frame 1) to middle anterolateral RA and splits into two wavefronts (frame 2); one passes through the gap (g) in the crista terminalis (CT) and activates superior posterolateral RA (frame 3), and the other passes through the lateral cavotricuspid isthmus. (B) Isopotential maps showing the activation sequence (frames 1 to 3) of atrial pacing after ablation. Color scale for each isopotential map has been set so that **white** indicates most negative potential and **blue** indicates least negative potential. The activation wavefront propagates downward from the superior anterior RA (frame 1) to middle anterolateral RA (frame 2) and splits into two wavefronts (frame 3); one passes around the cranial end of the CT and activates the superior posterior RA, and the other passes through the lateral cavotricuspid isthmus. L10 to L15 represent the radiofrequency ablation lesions. (C) Before ablation the virtual electrograms near the conduction gap in the CT demonstrate fractionated potentials. (D) After ablation the virtual electrograms near the conduction gap in the CT demonstrate double potentials, suggesting conduction block. IVC = inferior vena cava; SVC = superior vena cava.

Catheter ablation of atypical atrial flutter. For successful elimination of atrial flutter, the narrowest part of the re-entrant circuit is usually targeted for catheter ablation. Yang et al. (8) reported that RF ablation of the CTI with creation of bidirectional block was effective in eliminating lower loop re-entry tachycardia. Kall et al. (6) showed that RF energy application from a discrete midlateral RA central line of conduction block to the inferior vena cava terminated and prevented the reinduction of atypical atrial flutter in all six patients. In the present study the conduction gap in the crista terminalis was targeted for ablation. After ablation no atypical atrial flutter could be induced, and, during the follow-up period, no recurrence of atrial flutter and atrial fibrillation (in three patients) occurred. This finding suggested that the conduction gap in the crista terminalis is critical for maintenance of the re-entrant circuit of atypical atrial flutter and atrial fibrillation. In the canine sterile pericarditis model, sufficiently rapid atrial flutter on the RA free wall could degenerate into atrial fibrillation (20). Thus, the conduction gap in the crista terminalis may lead to breaks in the activation wavefront of upper loop re-entry and the formation of new “daughter” wavelets. After linear ablation of this gap, both arrhythmias disappeared.

Conclusions Atypical atrial flutter could arise from upper loop re-entry in the RA through the conduction gap in the crista terminalis. Radiofrequency linear ablation of the conduction gap was effective in eliminating this atrial arrhythmia.

Acknowledgment

The authors would like to thank Graydon Beatty of Endocardial Solutions, Inc., for his technical assistance with this study.

Reprint requests and correspondence: Dr. Ching-Tai Tai, Division of Cardiology, Department of Medicine, Taipei Veterans General Hospital, 201, Sec. 2, Shih-Pai Road, Taipei, Taiwan. E-mail: cttai@vghtpe.gov.tw.

REFERENCES

1. Olgin JM, Kalman JM, Fitzpatrick AP, Lesh MD. Role of right atrial endocardial structures as barriers to conduction during human type I atrial flutter: activation and entrainment mapping guided by intracardiac echocardiography. *Circulation* 1995;92:1839–48.
2. Kalman JM, Olgin JE, Saxon LA, Fisher WG, Lee RJ, Lesh MD. Activation and entrainment mapping defines the tricuspid annulus as the anterior barrier in typical atrial flutter. *Circulation* 1996;94:398–406.
3. Tai CT, Chen SA, Chiang CE, et al. Characterization of low right atrial isthmus as the slow conduction zone and pharmacological target in typical atrial flutter. *Circulation* 1997;96:2601–11.
4. Shah DC, Jais P, Haissaguerre M, et al. Three-dimensional mapping of the common atrial flutter circuit in the right atrium. *Circulation* 1997;96:3904–12.
5. Olgin JE, Jayachandran JV, Engesstein E, et al. Atrial macroreentry involving the myocardium of the coronary sinus: a unique mechanism for atypical atrial flutter. *J Cardiovasc Electrophysiol* 1998;9:1094–9.
6. Kall JG, Rubenstein DS, Kopp DE, et al. Atypical atrial flutter originating in the right atrial free wall. *Circulation* 2000;101:270–9.
7. Jais P, Shah DC, Haissaguerre M, et al. Mapping and ablation of left atrial flutters. *Circulation* 2000;101:2928–34.
8. Yang Y, Cheng J, Bochoeyer A, et al. Atypical right atrial flutter patterns. *Circulation* 2001;103:3092–8.
9. Tai CT, Chen SA, Chiang CE, et al. Long-term outcome of radiofrequency catheter ablation for typical atrial flutter: risk prediction of recurrent arrhythmias. *J Cardiovasc Electrophysiol* 1998;9:115–21.
10. Schilling RJ, Peters NS, Davies DW. A non-contact catheter for simultaneous endocardial mapping in the human left ventricle: comparison of contact and reconstructed electrograms during sinus rhythm. *Circulation* 1998;98:887–98.
11. Olshansky B, Okumura K, Henthorn RW, Waldo AL. Characterization of double potentials in human atrial flutter: studies during transient entrainment. *J Am Coll Cardiol* 1990;15:833–41.
12. Shimizu A, Nozaki A, Rudy Y, Waldo AL. Onset of induced atrial flutter in the canine pericarditis model. *J Am Coll Cardiol* 1991;17:1223–34.
13. Schoels W, Gough WB, Restivo M, El-Sherif N. Circus movement atrial flutter in the canine sterile pericarditis model: activation patterns during initiation, termination, and sustained reentry in vivo. *Circ Res* 1990;67:35–50.
14. Boyden PA. Activation sequence during atrial flutter in dogs with surgically induced right atrial enlargement. I. Observations during sustained rhythms. *Circ Res* 1988;62:596–608.
15. Schoels W, Kuebler W, Yang H, Gough WB, El-Sherif N. A unified functional/anatomic substrate for circus movement atrial flutter: activation and refractory patterns in the canine right atrial enlargement model. *J Am Coll Cardiol* 1993;21:73–84.
16. Tai CT, Chen SA, Chen YC, et al. Conduction properties of the crista terminalis in patients with typical atrial flutter: basis for a line of block in the reentrant circuit. *J Cardiovasc Electrophysiol* 1998;9:811–9.
17. Arenal A, Almendral J, Alday JM, et al. Rate-dependent conduction block of the crista terminalis in patients with typical atrial flutter: influence on evaluation of cavotricuspid isthmus conduction block. *Circulation* 1999;99:2771–8.
18. Schumacher B, Jung W, Schmidt H, et al. Transverse conduction capabilities of the crista terminalis in patients with atrial flutter and atrial fibrillation. *J Am Coll Cardiol* 1999;34:363–73.
19. Bharati S, Lev M. Histology of the normal and diseased atrium. In: Falk RH, Podrid PJ, editors. *Atrial Fibrillation: Mechanisms and Management*. New York, NY: Raven Press, 1992:15–39.
20. Ortiz J, Niwano S, Rudy YA, Johnson NJ, Waldo AL. Mapping the conversion of atrial flutter to atrial fibrillation and atrial fibrillation to atrial flutter: insights into mechanisms. *Circ Res* 1994;74:882–94.